

Large Eddy Simulation of Confined Circular Jet Opening in to a Rectangular Channel

G Dinesh Kumar Reddy
M.Tech, Aerospace Engineering
Indian Institute of Technology, Kanpur

Abstract

Turbulence is the most important parameter that enhances the mixing characteristics of the flow. This mixing process starts with the breaking of circular jet and its expansion. So, many researchers investigated the characteristics of a free circular jet at different Reynolds Numbers. The present study involves the numerical simulation of a confined circular jet opening in a rectangular channel using LES model. Smagorinsky - Lilly model is used for the present analysis which is capable of modelling the eddies well inside the core of the rectangular channel. Van driest damping model is used for better results near the walls. "pimpleFoam" (combination of piso and simple algorithm) solver is used. "OpenFoam", an open-source CFD toolbox, is used to analyse the expansion characteristics of the circular jet in a rectangular channel.

1 Introduction

A free jet is produced when fluid is ejected from the nozzle into an external ambient that can either be at rest or coflowing. In various engineering applications such as mixing, heating/cooling, printing, and propulsion, the mechanism driving the respective process depends on the evolution of the jet. Understanding flow physics in jets at different Reynolds numbers can improve the performance of the device. The jet evolution in the near field strongly depends on the inflow conditions. Far downstream the jet becomes fully turbulent but instabilities developing in the intermediate region govern the flow details.

There are different models (DNS, RANS, LES) to study the characteristics of the circular jet. Out of the 3 models DNS gives the most reliable results but the computational time and cost are so expensive. RANS gives the results that are not much reliable but computationally cheap. LES (Large Eddy Simulation) models the problem in such a way that the results are reliable and computationally effective. Smagorinsky Lilly model is one of the oldest and most used sub grid scale models.

2 Problem Statement

The main objective of the present work is to investigate the expansion characteristics of a confined circular jet expanding into a rectangular channel using Large Eddy Simulation in “openFoam” an opensource CFD toolbox. Fig[1] shows the schematic of the problem statement. The dimensions of the geometry are given in table 1. The analysis is done for different Reynolds numbers ranging from 1000 to 2000. The length of the geometry is variable and it has to be determined such that the flow should be fully developed for the chosen length of the geometry.

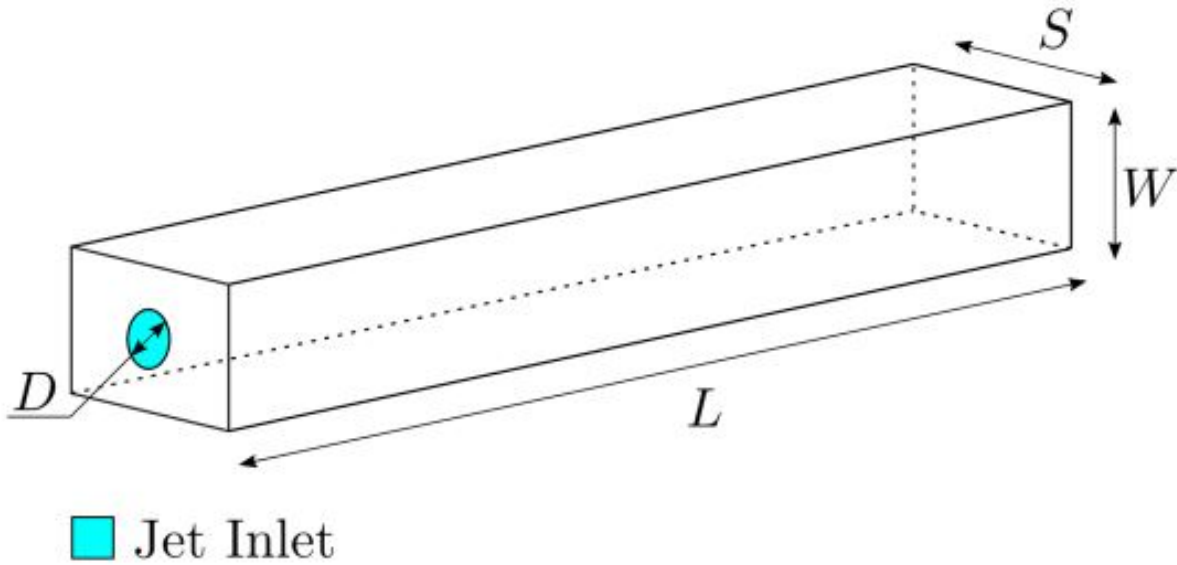


Figure 1: Schematic of problem statement

Table 1: Dimensions

Length-L(m)	Width-S(m)	Height-W(m)	Diameter-D(m)
Variable	0.04	0.01	5e-3

3 Governing Equations and Models

Equation 1 is the filtered Navier stokes equation which is the governing differential equation for the present analysis. The residuals in the filtered NS equation are modelled as extra shear terms (more viscosity ν_t in the subgrid scale). This differs from model to model. In Smagorinsky lilly model sub-grid scale viscosity is given by equation 2. S bar is the characteristic filtered rate of strain that has units same as $1/t$ and is used in the place of that in equation 2. Δ is turbulent length scale which is used to differentiate the eddies i.e., the eddies that are smaller than Δ are modelled as increase in viscosity.

$$\frac{\overline{D}\bar{u}}{\overline{D}t} = \nu \frac{\partial^2 \bar{u}_i}{\partial x_i \partial x_i} + \frac{\partial}{\partial x_i} \nu_t \left(\frac{\partial \bar{u}_j}{\partial x_j} + \frac{\partial \bar{u}_i}{\partial x_j} \right) - \frac{1}{\rho} \frac{\partial \bar{p}}{\partial x_j} \quad (1)$$

$$\nu_t = l_{characteristic}^2 * \frac{1}{t} \quad (2)$$

$$\bar{S} = \sqrt{2S_{ij}S_{ij}} \quad (3)$$

$$S_{ij} = \frac{1}{2} \left(\frac{\partial \bar{u}_i}{\partial x_j} + \frac{\partial \bar{u}_j}{\partial x_i} \right) \quad (4)$$

$$\nu_t = l_{characteristic}^2 * \bar{S} \quad (5)$$

$$l_{characteristic} = \Delta * C_{smagorinsky} \quad (6)$$

Near the wall, the eddies will be so small and so in order to solve those eddies finer mesh is required. This in turn increases the computational time and power. In smagorinsky model turbulent viscosity is constant. So, to resolve smaller eddies near the walls, a finer mesh is needed. So, using a variable turbulent viscosity, one can solve the smaller eddies without refining the mesh.

$$l_{characteristic} = \Delta * C_s (1 - e^{-\frac{y^+}{A^+}}) \quad (7)$$

$$\Delta_g = \frac{l_{characteristic}}{C_s} = V^{\frac{1}{3}} \quad (8)$$

$$\Delta = \frac{k * y}{C_s} (1 - e^{-\frac{y^+}{A^+}}) \quad (9)$$

$$\Delta = \min\left(\frac{k * y}{C_s} (1 - e^{-\frac{y^+}{A^+}}), \Delta_g\right) \quad (10)$$

4 Simulation Procedure

4.1 Geometry and Mesh

”blockMesh” utility which is an in-built modelling and mesh generation utility in ”openFoam” is used to both model and mesh the geometry. Lien et al. (2004), recommended the length of the channel to be 150 times the height of the channel for the flow to get fully developed. So, a length of 1.5m is taken as the channel length. The geometry is divided into 9 blocks in order to get the required mesh. X axis is taken as the flow direction(along the length), Y axis is taken as the wall normal direction(along the height) and Z axis is taken as the cross stream direction(along the span). To create the mesh required for the Large Eddy Simulation ”kolmogorov” length scale is taken as reference. For DNS simulations the height of the first cell near the wall is given by the equation 11, where eta is the first cell height, l is the reference length or the characteristic length(in the present case ”height”), Re is the Reynolds Number.

$$\frac{\eta}{l} = Re^{-\frac{3}{4}} \quad (11)$$

But for LES it’s not necessary to resolve small eddies. So, the following approach is followed to get the required mesh. Equation is the Blasius equation gives the coefficient of friction which is applicable for internal flows. Friction velocity is calculated from the shear stress. Equation 15 is used to get the first cell height in each direction.

$$C_f = 0.079 * Re^{-\frac{1}{4}} \quad (12)$$

$$\tau_w = \frac{1}{2}\rho U^2 C_f \quad (13)$$

$$u_\tau = \sqrt{\frac{\tau_w}{\rho}} \quad (14)$$

$$\Delta x = \frac{\Delta x^+ \nu}{u_\tau} \quad (15)$$

For this LES simulation y^+ of 2 and x^+ of 20 is taken such that the mesh aspect ratio lies below 25. The analysis is done for 2 different cases periodic and confined. For the periodic case the span-wise direction is taken as periodic and so, z^+ of 20 is used. For the later case where the z-axis is also wall normal direction so, z^+ of 2 is used. The mesh details are given in the table below.

Table 2: Grid Details for Periodic Case

Reynolds Number	Divisions along each axis	No. of cells	x^+	y^+	z^+
1000	540x19x36	369360	20	2	20
2000	568x23x48	627072	20	2	20

Table 3: Grid Details for confined Case

Reynolds Number	Divisions along each axis	No. of cells	x^+	y^+	z^+
1000	540x19x48	4,92,480	20	2	2
1200	560x20x50	5,60,000	20	2	2
1500	560x21x58	5,82,080	20	2	2
1800	563x23x64	8,28,736	20	2	2
2000	568x23x74	9,66,736	20	2	2

4.2 Initial and Boundary Conditions

Gohil et al.(2012) discussed the importance of the inlet perturbations required to induce turbulence at the inlet. Poletto et al. (2013) suggested that the inlet perturbations decreases the flow development length there by reducing the computational cost and time. At first, a nonuniform inlet type is used where the velocity fluctuations vary as a fourth order curve from bottom wall to top wall. But, no improvement in flow length is observed. Next tried with a different type of inlet called ‘‘turbulentDFSEMInlet’’ for which more input data that is acquired from other simulations is needed which increases the both computational cost and time. Finally, gaussian perturbation method is used as suggested in [1] and the code for those perturbations is obtained from [4]. Fig 1 shows the velocity distribution at the inlet on the channel. The cell data at the inlet is extracted using ‘write-CellCentres’ function in openFoam. The perturbations in each direction are calculated from the code [4] and a mean velocity is added to the perturbations in stream wise direction and all the three velocities are merged into a single file using Octave and is given as input to the ‘U’ file in ‘0’ folder. The code used for getting the velocity fluctuations is given below.

```
// Gaussian random points in plane

// usage:  gaussian_points -N #

// Michel Vallieres

// Code is needed for randomization of velocity distribution

// ***** End Note *****

#include <stdio.h>
#include <stdlib.h>
#include <math.h>

// uniform random #s in [0,1]
// rand() is a c library code, the variable is uniformly distributed

// ***** define global variables *****//

double gauss1, gauss2;
void gaussian_rand();

double rand01()

{
//srand(time(0));
return (double)rand()/(double)RAND_MAX;
}

// gaussian random # with <x>=1 & sigma=1
// Koonin & Meredith, 1990

//double gaussian_rand()
void gaussian_rand()
{
//double twou, radius, theta, gauss1, gauss2;
double twou, radius, theta;
double unrand01;

unrand01 = rand01();
// printf("%lf \n", unrand01);
twou = -2.0 * log (1.0 - rand01() );
radius = sqrt( twou );
theta = 2 * M_PI * rand01();
gauss1 = radius * cos(theta);
gauss2 = radius * sin(theta);
```

```
// return gauss1;
return;
}

int main( int argc, char * argv[] )
{

FILE *fout;

int i;
int N;

double M, sigma;

printf("Type the value of mean (M): \n");
scanf("%lf", &M);
printf("Read the value of mean (M):%lf \n", M);
printf("Type the value of sigma (sigma):\n");
scanf("%lf", &sigma);
printf("Read the value of sigma (sigma):%lf \n", sigma);

N = 20;
if ( argc == 3 )
    if ( argv[1][0] == '-' && argv[1][1] == 'N' )
        N = atoi( argv[2] );

fout = fopen("./RanData.txt","w+");
for ( i=0; i<N; i++ )
{
    //printf( "%f %f \n", gaussian_rand(), gaussian_rand() );
    gaussian_rand();
    fprintf( fout, "%f      %f \n", sigma*gauss1+M, sigma*gauss2+M );
}
fclose(fout);
}
```

4.2.1 Numerical Boundary Condition

Using Smagorinsky model to simulate the problem, only three parameters is needed to be described which are velocity (U), kinematic pressure (p) and turbulent kinematic viscosity (ν_t).

Table 4: Boundary conditions for 'U'

Patch	Condition	Value(m/s)
Inlet	Non- uniform velocity vector	-
Outlet	Zero-Gradient	-
Top and Bottom	Fixed value	(0 0 0)
Front and Back	symmetric	-

Table 5: Boundary conditions for 'P'

Patch	Condition	Value(N/m ²)
Inlet	Zero-Gradient	-
Outlet	Fixed value	0
Top and Bottom	Zero-Gradient	-
Front and Back	symmetric	-

Table 6: Boundary conditions for 'nut'

Patch	Condition	Value(Ns/m ²)
Inlet	Zero-Gradient	-
Outlet	Zero-Gradient	-
Top and Bottom	Zero-Gradient	-
Front and Back	symmetric	-

Table 7: Initial Boundary Conditions

Sl. No	Channel Based Reynolds Number	Cross Sectional Area Averaged Velocity(m/s)	Jet inlet velocity(m/s)	Dynamic Viscosity (Ns/m ²)	Density (Kg/m ³)
1	1000	1	20.37	1e-5	1
2	2000	2	40.74	1e-5	1

4.3 Solver

Large Eddy Simulation resolves the biggest eddies which tend to carry most of the momentum, heat and energy and models the smallest eddies. Even though the smallest eddies dissipate more energy but the energy lost is very less because they don't carry most of the momentum. So, LES is computationally efficient compared to Direct Numerical Simulation which resolves all the eddies from big to small. PimpleFoam solver is used for the present analysis which is more robust and efficient. It can be used for larger time steps (compared to piso, where courant number greater than 1 result in diverged simulation). Pimple offers more control by providing outer iterations that could

improve the results, whereas when `nouterCorrectors = 1` pimple is just simply a piso algorithm.

Step 1: The momentum equations are solved from the assumed pressure p which yields the velocity field.

Step 2: The pressure equation is solved using obtained velocity field.

Step 3: Velocity fields are corrected that is obtained from Step 2. 2 and 3 steps act as corrector loop also called innerCorrectors in "openFOAM".

Step 4: The turbulence related fields are then corrected. Those fields are again used to solve momentum equation on step 1 and looped until desired residual tolerance criteria are met. This is known as pressure velocity coupling or outerCorrectors.

Step 5: Forward time marching until end time.

```
PIMPLE
{
    nNonOrthogonalCorrectors 1;
    nCorrectors 1;
    nOuterCorrectors 50;

    residualControl
    {
        U
        {
            tolerance 1e-4;
            relTol 0;
        }
        p
        {
            tolerance 5e-3;
            relTol 0;
        }
    }
}

relaxationFactors
{
    equations
    {
        ".*" 1;
    }
}
```

Table 8: Numerical Solvers

Field	Solver	Smoother	Tolerance
U	Smooth solvers	Gauss Seidel Smoother	1e-6
P	GAMG solver	Gauss Seidel Smoother	1e-5
nut	Smooth solvers	Gauss Seidel Smoother	1e-6

4.4 Domain Optimization

As the width and height of the channel are fixed from the experimental domain, simulations are carried out for periodic case at Re 2000 for optimizing the length of the channel. Since the spanwise direction is periodic, in order to reduce the computational time, the channel width is reduced to 10mm and the simulations are carried out. At first the channel length is taken as 300mm and the simulations are carried out for 6s and the results are as follows.

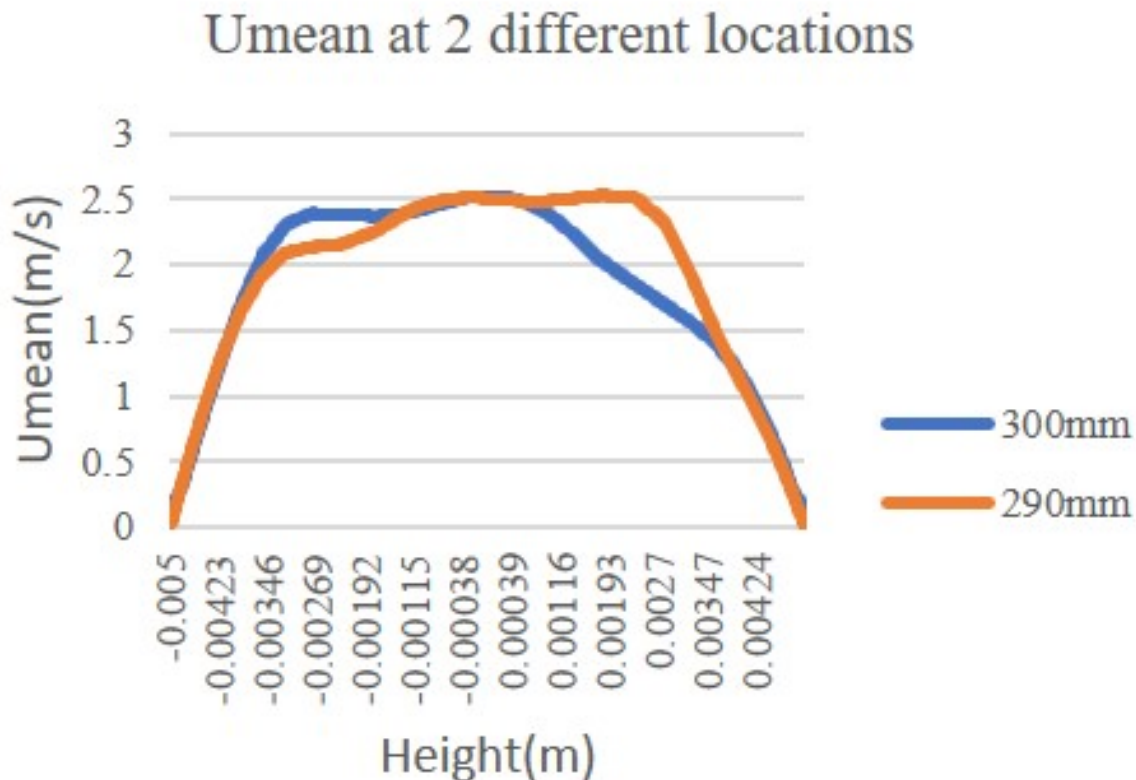


Figure 2: Caption

From fig 2 it is observed that the Umean at 2 different locations downstream is not overlapping which shows that the flow has not attained the Self similarity. The analysis is continued for the length of 1000mm length and for a run time of 6s and the results are as follows

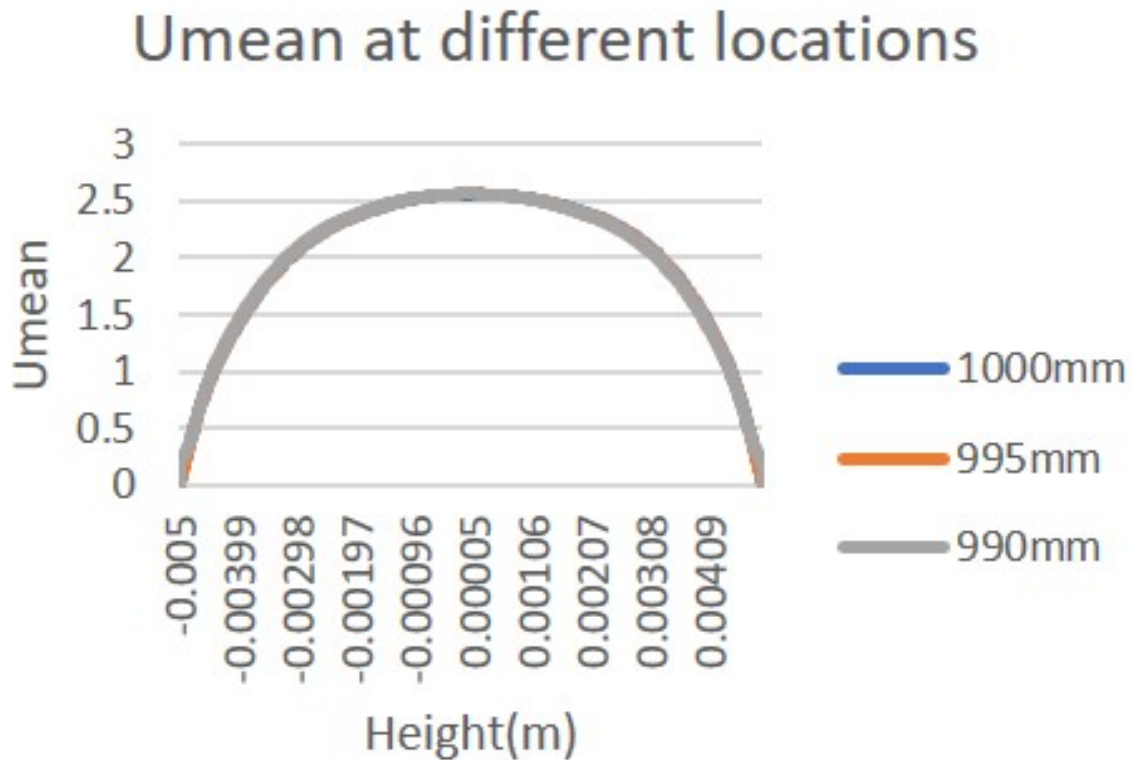


Figure 3: Caption

From fig 3 it is observed that the U_{mean} at 2 different locations downstream is not overlapping which shows that the flow has attained the Self similarity. So, a length of 1m is taken as the channel length for the periodic case.

5 Results and Discussions

Time convergence and Spatial convergence tests are conducted for both the periodic and confined cases. The maximum courant number is taken as 1 such that the Pimple algorithm takes the time step accordingly.

5.1 Mean Velocity Profiles

Plot over line utility in paraview is used to get the data of the mean velocity variation along the height of the channel. To check the spatial convergence the data is extracted at 3 different downstream locations i.e., at $x=1.44m$, $1.46m$ and $1.48m$ when $t=5s$. The velocity vs y/D data is plotted and are as shown in fig. Also to check the temporal convergence mean velocity data is extracted at 3 different time steps i.e., at $t=4.8s$, $4.9s$, $5s$ where $x=1.48m$. The velocity vs y/D is plotted and are shown in fig 4.

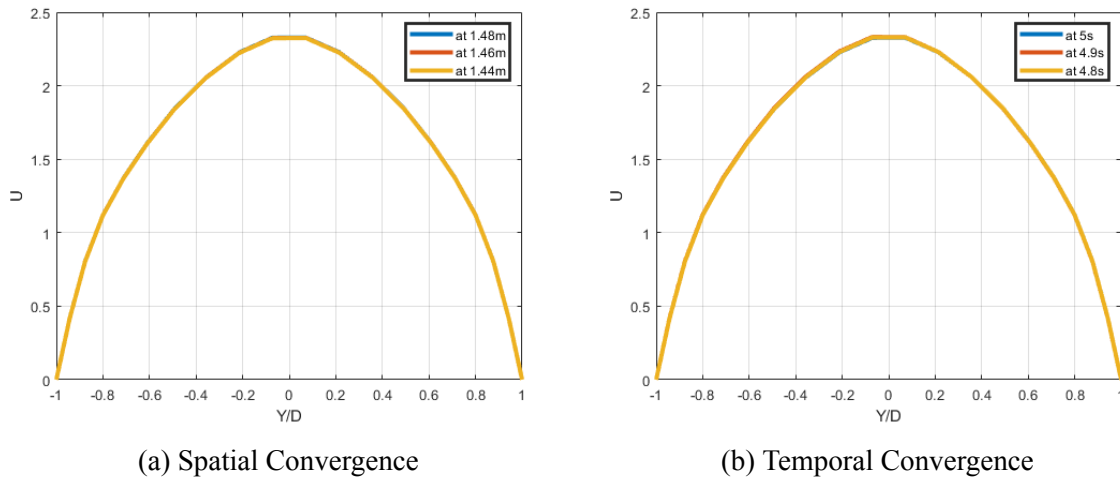


Figure 4: Mean velocity profiles to check the Spatial and Temporal convergence

From the plots it is observed that the curves at different downstream locations are getting overlapped which suggests that Spatial convergence is attained. Also, the plots are overlapped for different time steps. So, temporal convergence is also attained. So, for Re 1000 the convergence criteria is full-filled. The velocity curve follows parabolic path. Also the maximum velocity attained in the channel is 1.5 times the mean velocity. These are the properties of a laminar flow profile. So, it can be concluded that the flow is laminar at 1000 Reynolds Number. Similar spatial and temporal convergence studies are carried out for the Reynolds Numbers 1200, 1500, 1800, 2000. The plots are given in Appendix.

5.2 Rms Velocity profiles

In the previous section the convergence criteria for the mean velocities is discussed. Since, instantaneous velocity is a combination of mean and fluctuation components, it is necessary to study the fluctuating components. These fluctuating components are given in terms of stress tensors called Reynolds stresses $\langle u'u' \rangle$, $\langle v'v' \rangle$ and $\langle w'w' \rangle$ which are the principal diagonal terms in the stress tensor. These Reynolds stress tensors are averaged using fieldAverage function in controlDict file. The averaging starts after 0.6s of simulation time at which a steady nature in velocity signals is observed so that mature results will be obtained. Rms velocities are the square root of these principal diagonal terms. They are calculated using the in-built calculator in paraView. The Rms velocities are normalized with mean velocity and are plotted against y/D at 3 different downstream locations at $t=5s$ and at 3 different time steps at $x=1.48m$ as shown in fig 6.

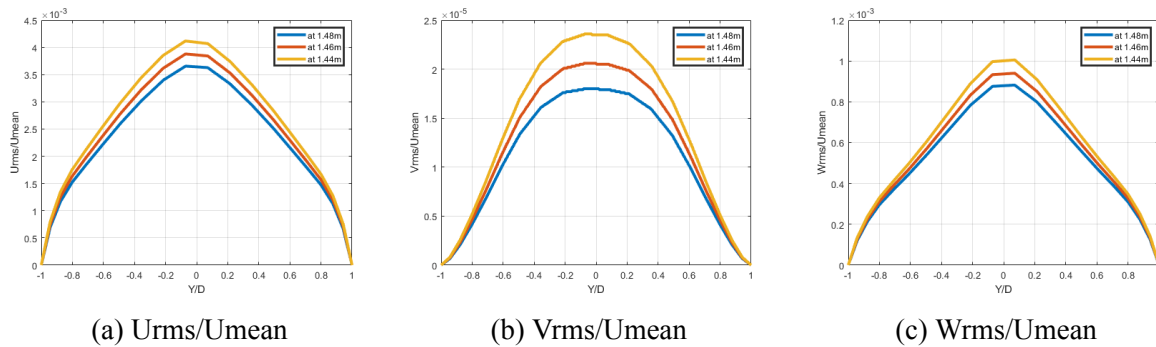


Figure 5: Spatial Convergence of Rms velocity profiles for Re 1000

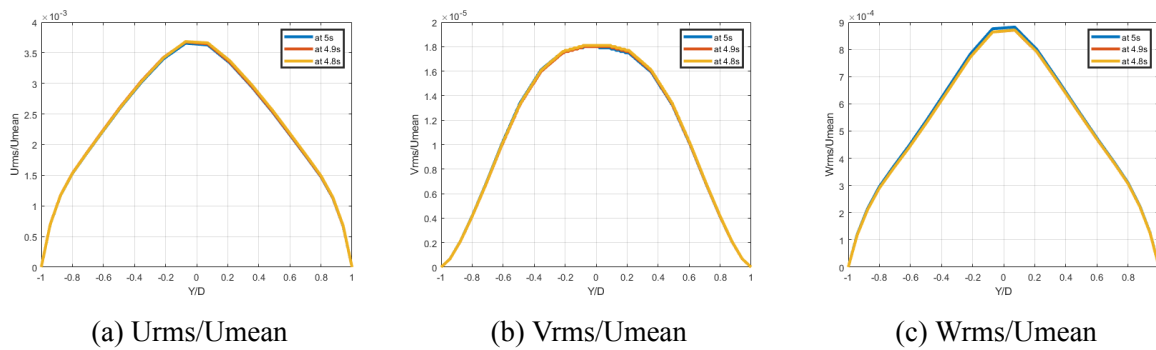


Figure 6: Temporal Convergence of Rms velocity profiles for Re 1000

5.3 Turbulent Shear Stresses

The non-diagonal stress tensors are known as the shear stresses which have same units as stress. They are $\langle u'v' \rangle$, $\langle v'w' \rangle$, $\langle u'w' \rangle$ and are calculated from the UPrime2MeanXY, UPrime2MeanYZ and UPrime2MeanXZ. They are normalized using square of mean velocity and are plotted against y/D at different downstream locations and different time steps as shown in fig 7

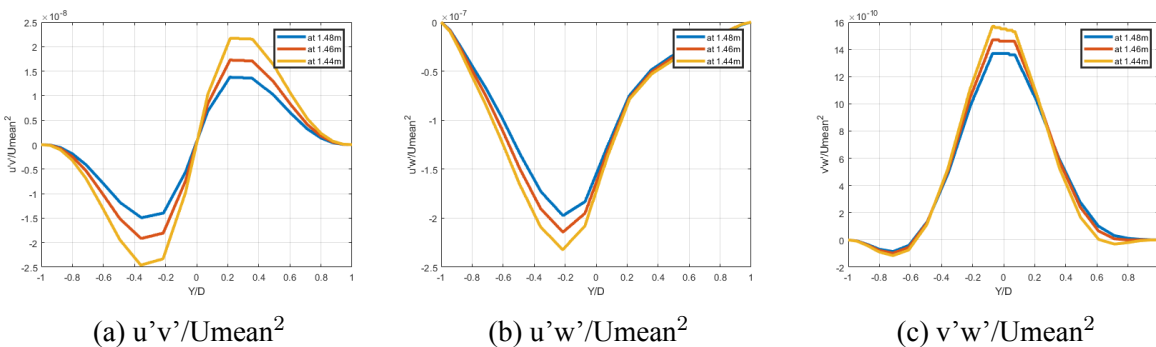


Figure 7: Spatial Convergence of turbulent shear profiles for Re 1000

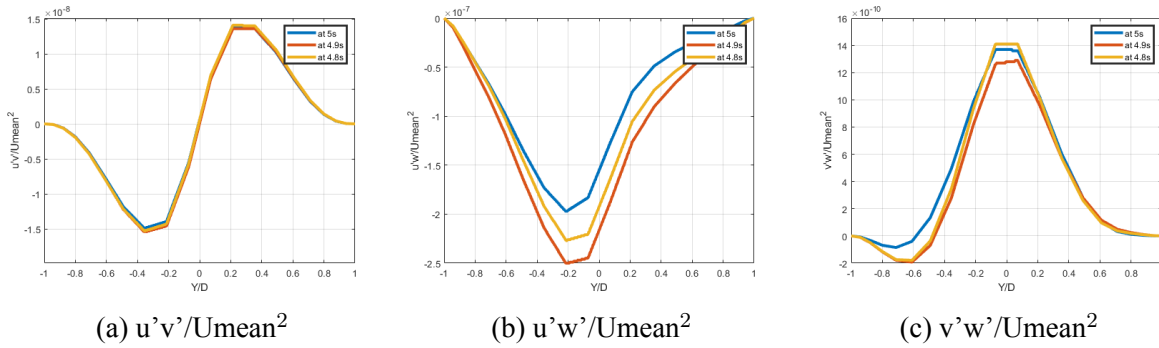


Figure 8: Temporal Convergence of turbulent shear profiles for Re 1000

5.4 Turbulent Kinetic Energy

The dissipation of kinetic energy depends on the size of the eddies. Larger eddies dissipate more energy at a slower rate and smaller eddies dissipate a very least amount of kinetic energy as they carry less energy which is negligible. So, the turbulent kinetic energy contours are one of the important parameters to check the turbulence in the flow. So, the turbulent kinetic energy contours are extracted at 3 different downstream locations i.e, at $x=0.01m$, $0.75m$, $1.49m$ and are as shown in fig 9.

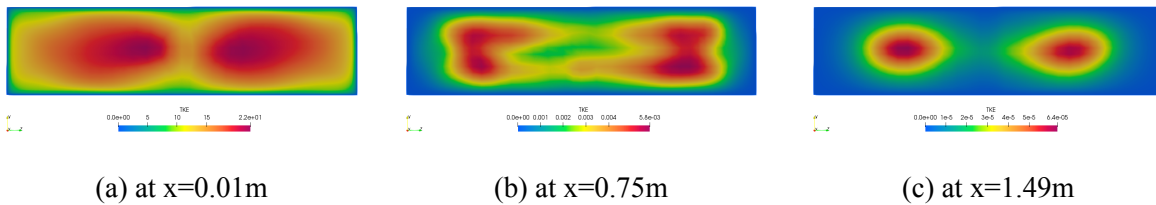


Figure 9: Turbulent Kinetic Energy contours for Re 1000

As we can see the magnitude of turbulent kinetic energy is more at $x=0.01m$ which is basically very near to the inlet of the circular jet where the flow should be turbulent. As we move downstream the turbulent kinetic energy magnitude is getting decreased. This is evident that the eddies are getting died out in the downstream and the flow is laminar. The turbulent kinetic energy contours for 1200, 1500, 1800, 2000 Re are given in Appendix-A.

5.5 Secondary Flows

As the flow is in the x direction and there is no any velocity magnitudes added in the other directions except the perturbations which gets died out in the downstream, there should not be any flow in the cross stream and wall normal direction for the laminar flow. So, based on the magnitude of secondary flow we can decide whether the flow is laminar or turbulent. So, using the calculator in parview the secondary flow magnitude is calculated using the formula " $U_y * jHat + U_z * kHat$ "

at 3 different downstream locations as shown in fig 10.

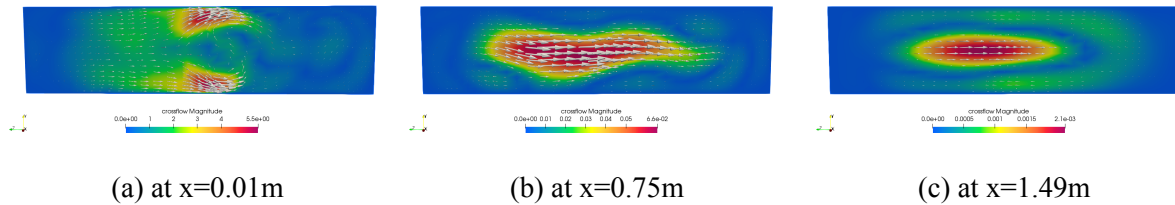


Figure 10: Secondary flow contours for Re 1000

The magnitude of cross flow is more near the inlet which suggests that the flow is turbulent and it is getting decreased as we move downstream. The arrows in the contours define the direction of the flow in that cross section. At the inlet the arrows are aligned in different direction but in the downstream they are getting aligned only in a single direction. This shows that the flow is laminar at Re 100.

5.6 Q-criterion

Q-criterion defines vortices as areas where the vorticity magnitude is greater than the magnitude of the rate of strain. So, it is one of the important methods to see turbulence inside the channel. The fig.11 shows the isosurfaces of Q-criterion for a value of 500.

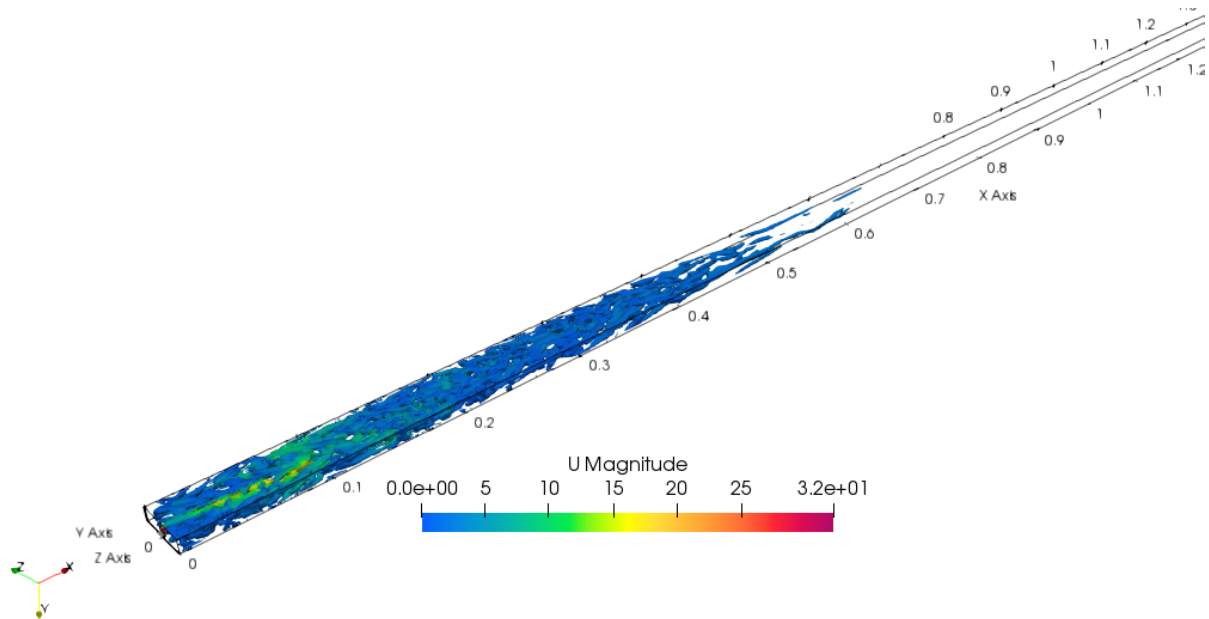


Figure 11: Iso-surface of Q-Criterion for Re 1000

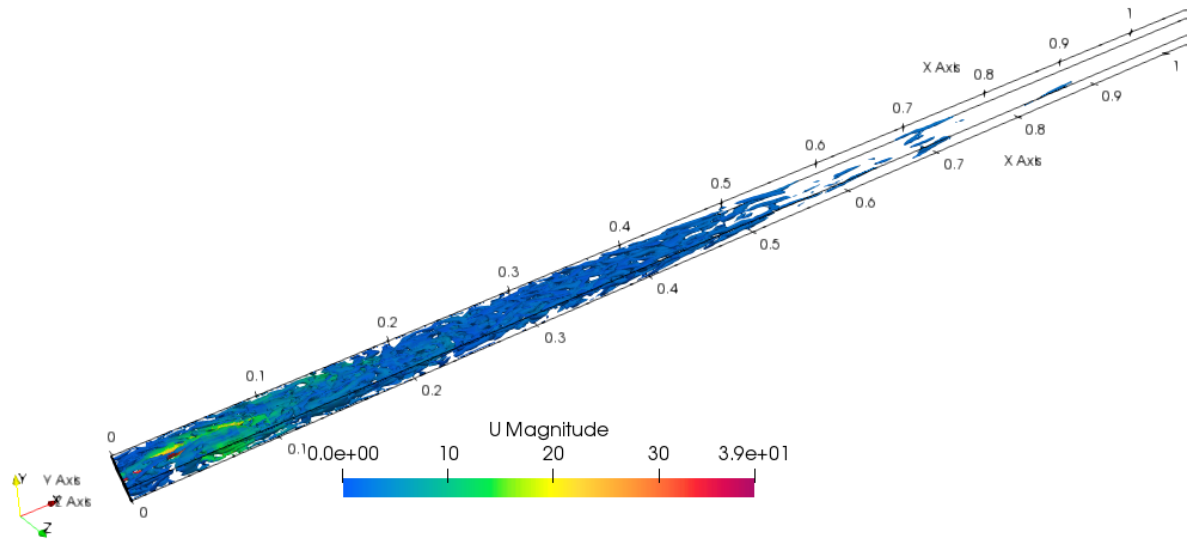


Figure 12: Iso-surface of Q-Criterion for Re 1200

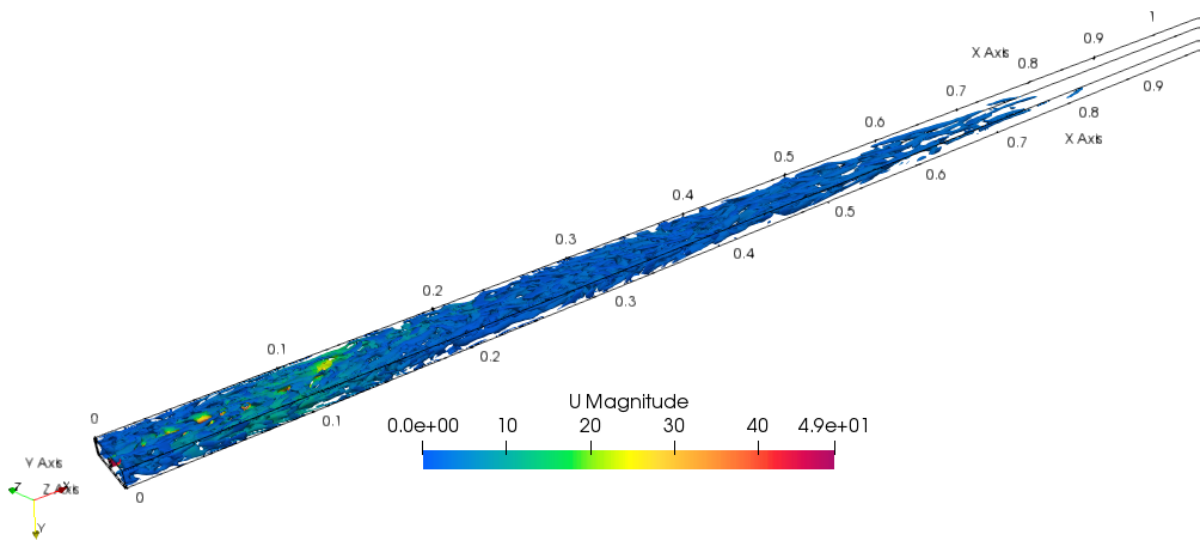


Figure 13: Iso-surface of Q-Criterion for Re 1500

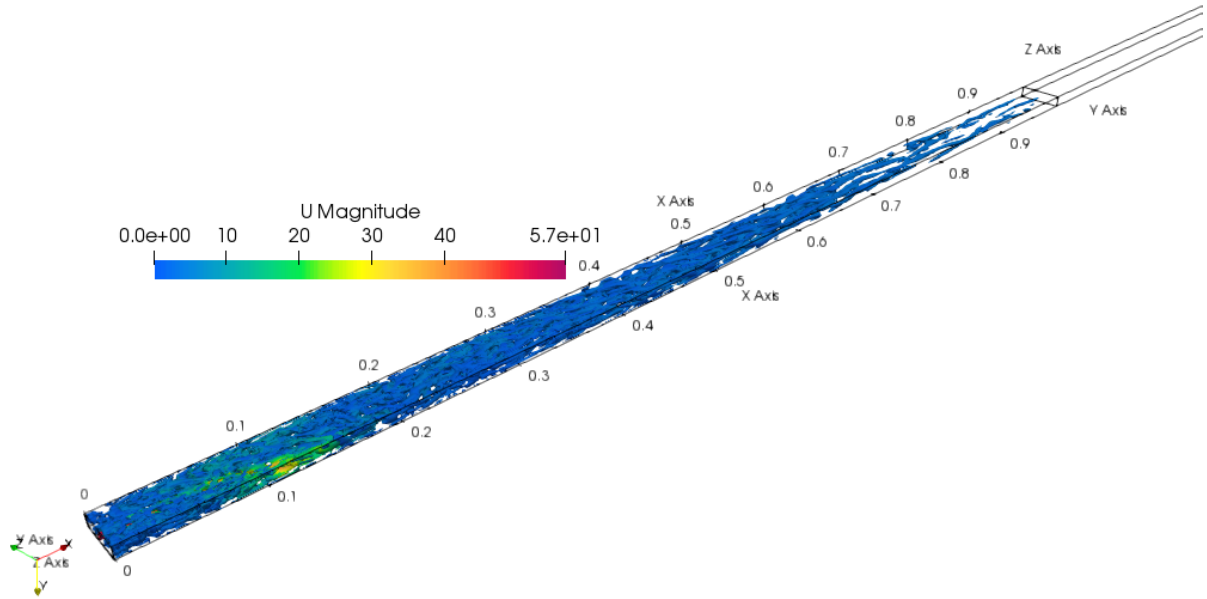


Figure 14: Iso-surface of Q-Criterion for Re 1800

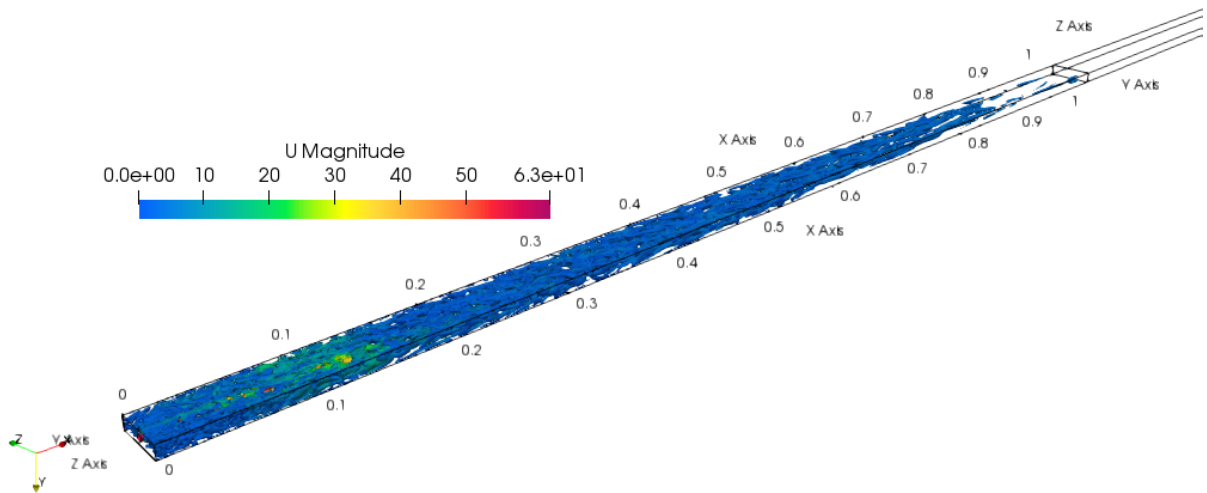


Figure 15: Iso-surface of Q-Criterion for Re 2000

From the above figures it is observed that the vortices inside the channel extends to the exit of the channel as the Reynolds number increases.

5.7 Comparison between Periodic and Confined cases

Fig 16 shows the comparison of the streamlines in the x-z plane for between periodic case and confined case at a Reynolds number of 1000.

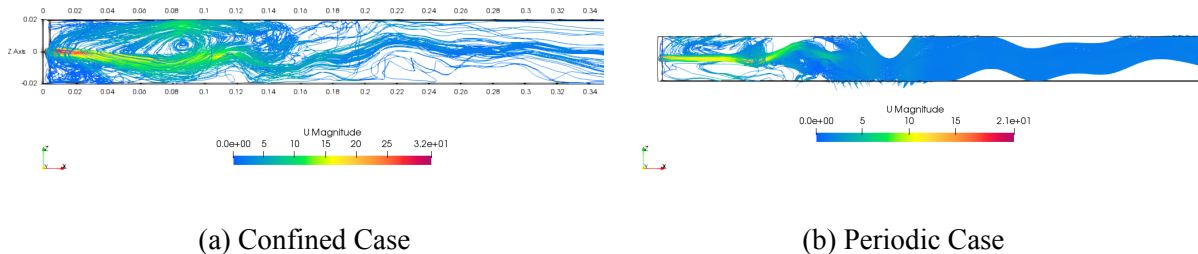


Figure 16: Stream lines for periodic and confined cases

From the fig it is observed that there is a re-circulation zone created in the case of confined geometry but there is no re-circulation zone being created in the case of Periodic. There is no wall in the z direction in the periodic case so there will not be any wall effects on the flow like the boundary layer effect. In the confined case where there is a wall in z-direction, there will be boundary layer formation. This boundary layer creates the re-circulation zone because of the velocity difference between the edge of the boundary layer and the circular jet.

6 Conclusions

It is observed that the the velocity fluctuations attain steady behaviour after 0.6s of simulation time. So, the Reynolds stresses starts averaging after 0.6s to obtain mature results. From the convergence plots as shown in Appendix ... it is observed that the temporal convergence occurred after 5s of simulation time. The Umean is converged spatially in ally the cases but the Rms velocities and the turbulent stresses seems to deviate from one another in all the cases. Also, the magnitude of the velocity fluctuations is very very less compared to Umean and so the deviation occurs in them. So, it can be concluded that the flow becomes self similar with in a length of 1.5m for the confined case and with in a length of 1m for the periodic case.

The re-circulations zones are being created in the x-z plane because of the boundary layer effect getting introduced by the wall. This plays a major role in breaking up of the circular jet. The re-circulation zone is not created in the periodic case as there is no wall in the z direction. From the Appendix.... it is observed that the length of the re-circulation zone is getting increased with Reynolds Number.

The Secondary flows are getting introduced as the Reynolds number increases. This is evident for the turbulence being induced is getting increases with increase in Reynolds number. The turbulent kinetic energy is increasing with Reynolds Number. Since, the larger eddies carries more kinetic energy and dissipate this increase in turbulent kinetic energy suggests that there are eddies

in the channel and the number of eddies are increasing with Reynolds number which is shown in Appendix-A. From Appendix-C it is evident that the jet is oscillating the x-z plane. This is because of the re-circulation zone being shifted from left to right. This shift in re-circulation zone is due to the z-component of velocity fluctuation being varying with time.

Acknowledgement

I would like to express my sincere gratitude and respect towards Prof. Manaswita Bose, IIT Bombay for constantly supporting and guiding me till the completion of project in the internship. Also, I am very thankful to Mr. Ashley Melvin and Mr. Divyesh Variya for helping me out with every doubts and problems which I had to tackle on this period. I am grateful towards the lab computers facility at IIT, Bombay, for providing access to its High Performance Computing facilities without which I wouldn't be able to complete my project.

Appendix-A

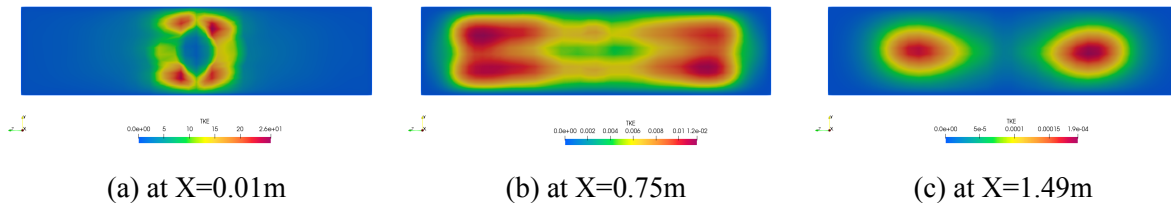


Figure 17: Turbulent Kinetic Energy contour for Re 1200

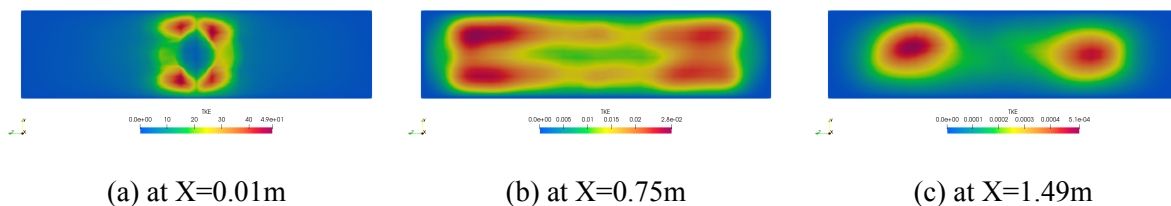


Figure 18: Turbulent Kinetic Energy contour for Re 1500

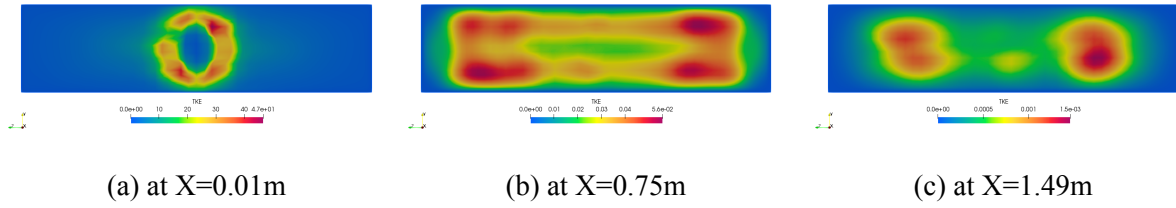


Figure 19: Turbulent Kinetic Energy contour for Re 1800

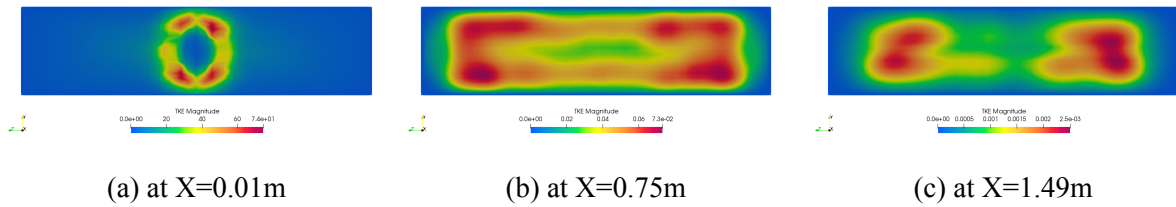


Figure 20: Turbulent Kinetic Energy contour for Re 2000

Appendix-B

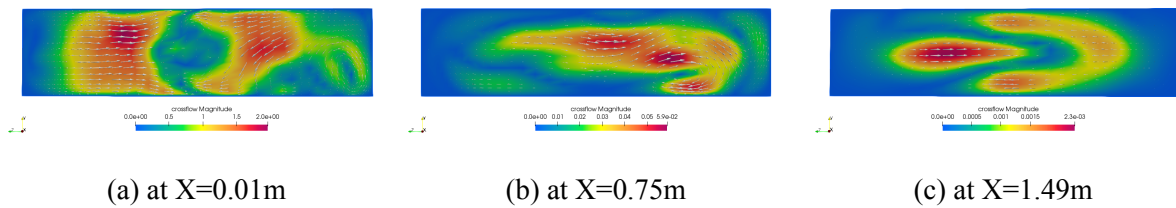


Figure 21: Cross Flow contour for Re 1200

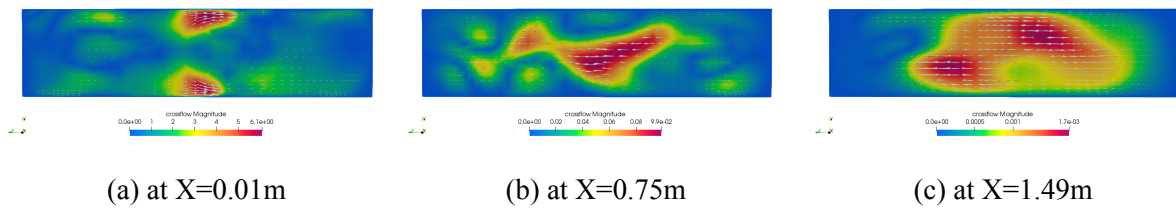


Figure 22: Cross Flow contour for Re 1500

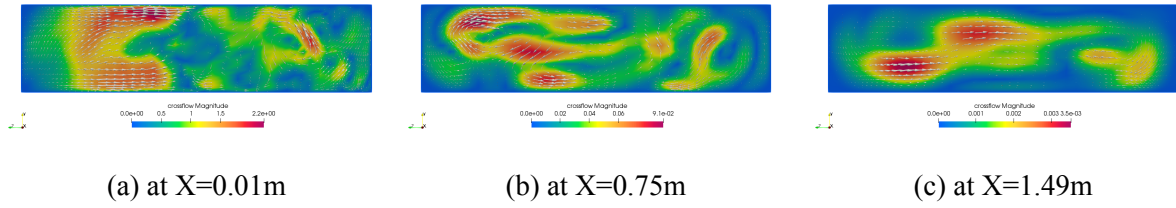


Figure 23: Cross Flow contour for Re 1800

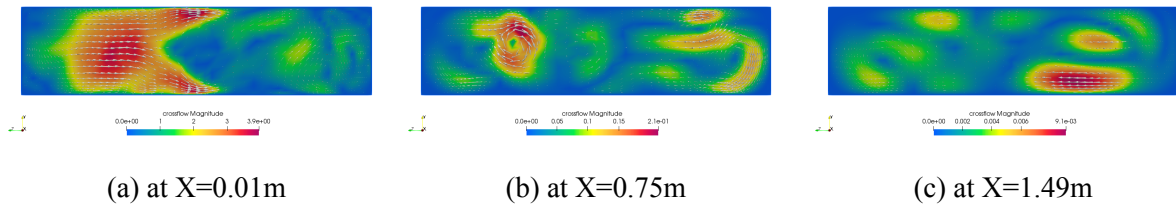


Figure 24: Cross Flow contour for Re 2000

Appendix-c

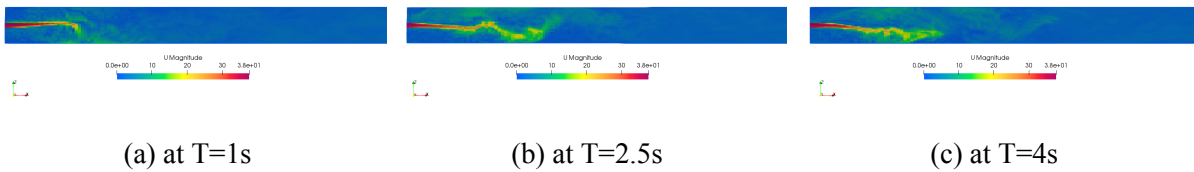


Figure 25: Velocity Contours in X-Z plane at different time steps for 1200 Re

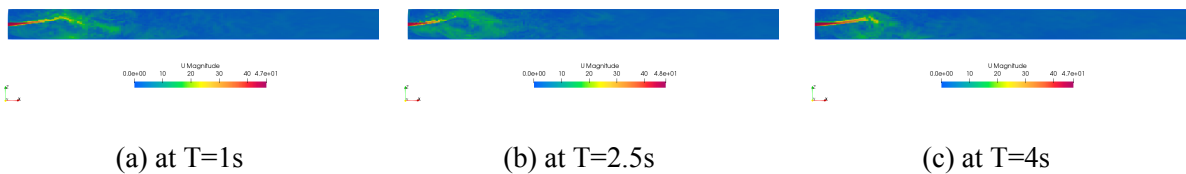


Figure 26: Velocity Contours in X-Z plane at different time steps for 1500 Re

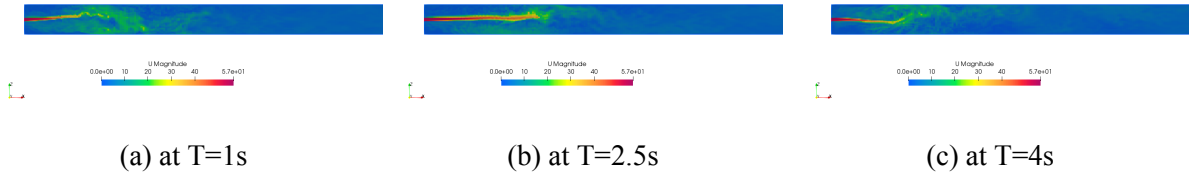


Figure 27: Velocity Contours in X-Z plane at different time steps for 1800 Re

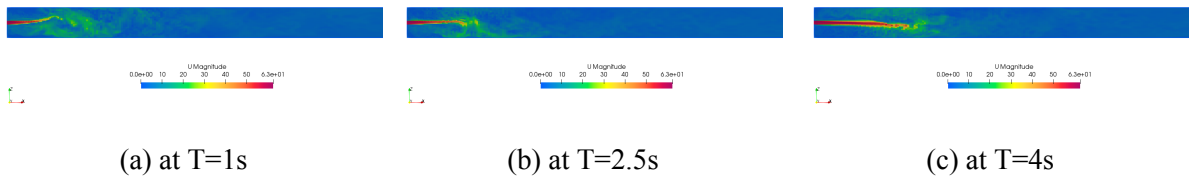


Figure 28: Velocity Contours in X-Z plane at different time steps for 2000 Re

Appendix-D

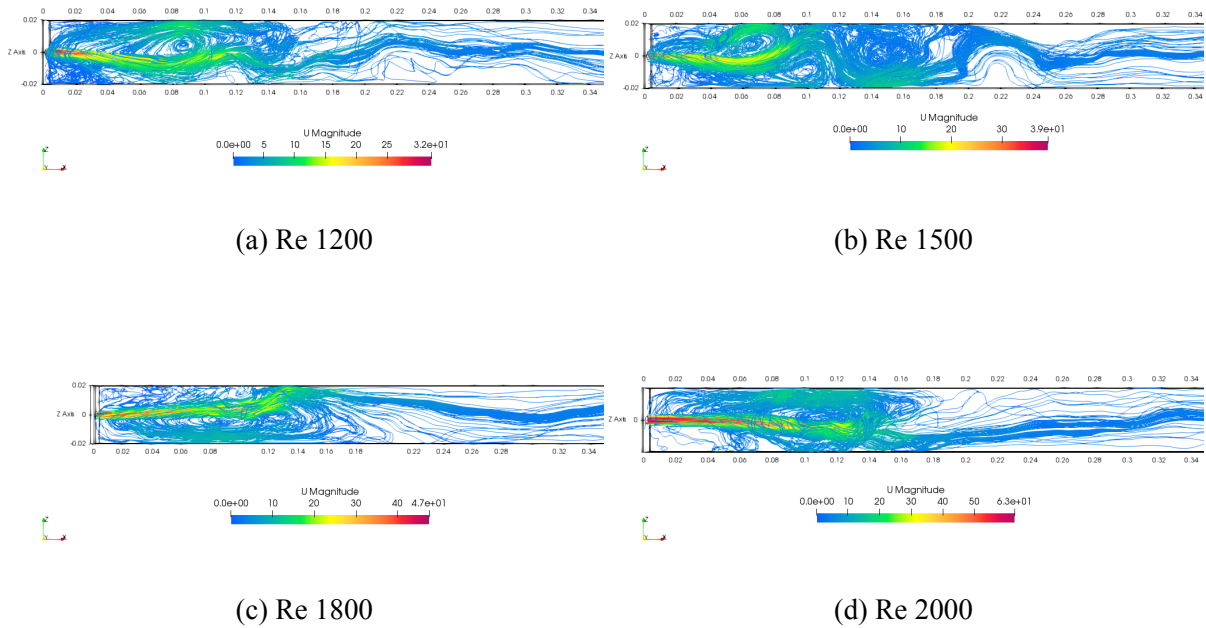
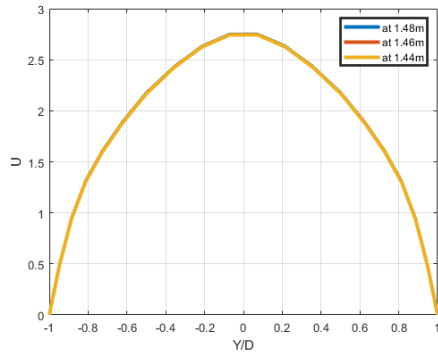
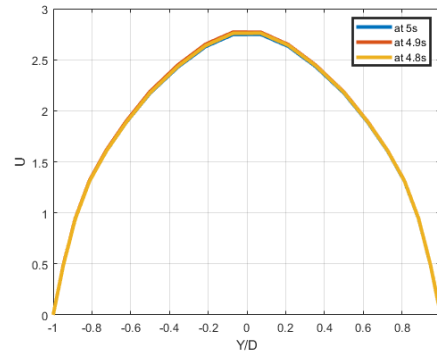


Figure 29: Stream lines contours for different Reynolds Numbers

Appendix-E

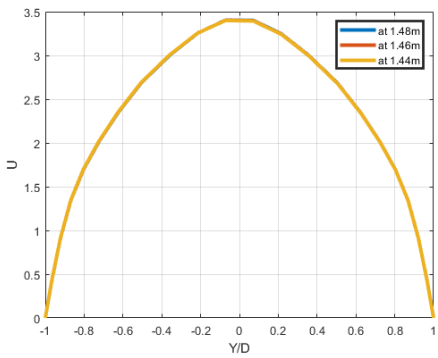


(a) Spatial convergence

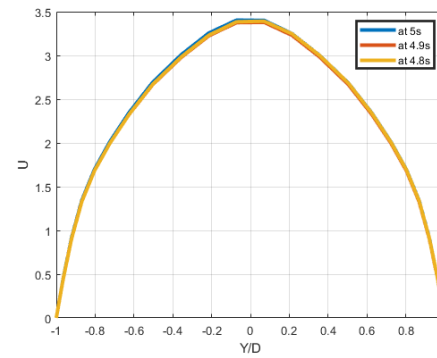


(b) Temporal convergence

Figure 30: Mean Velocity profiles for Re 1200

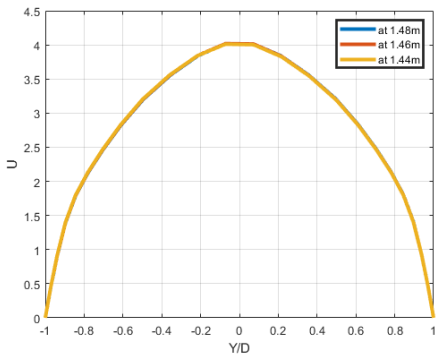


(a) Spatial convergence

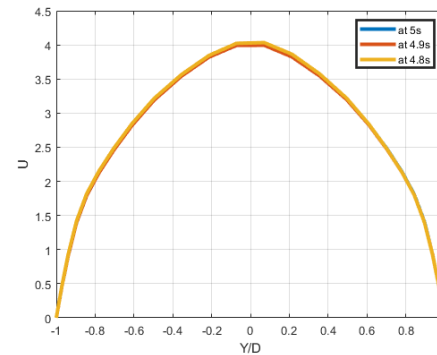


(b) Temporal convergence

Figure 31: Mean Velocity profiles for Re 1500



(a) Spatial convergence



(b) Temporal convergence

Figure 32: Mean Velocity profiles for Re 1800

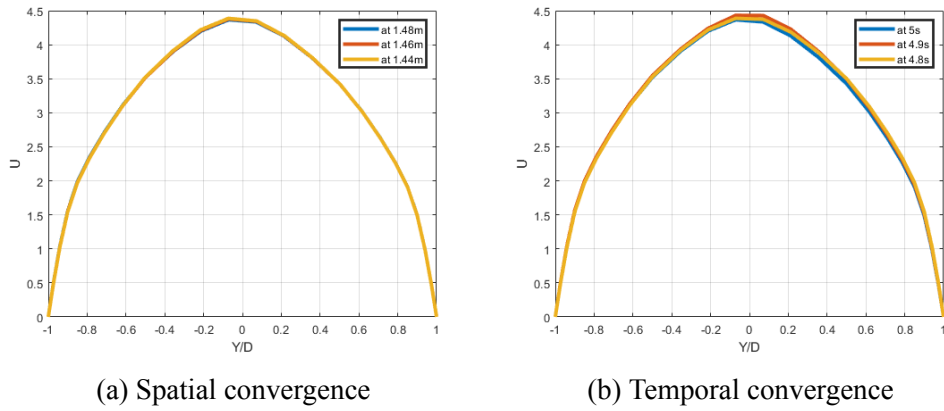


Figure 33: Mean Velocity profiles for Re 2000

Appendix-F

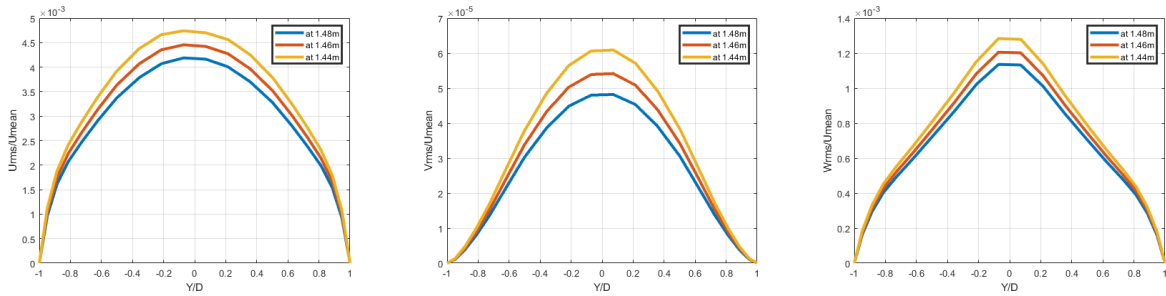


Figure 34: Spatial convergence of Rms Velocity profiles for Re 1200

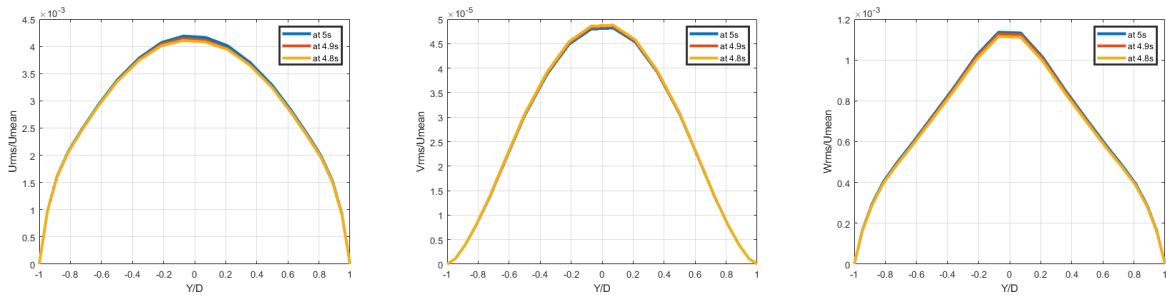


Figure 35: Temporal Convergence Rms Velocity profiles for Re 1200

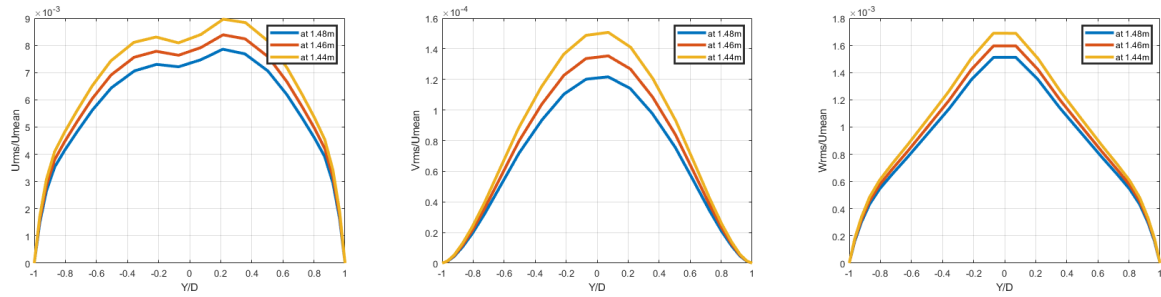


Figure 36: Spatial convergence of Rms Velocity profiles for Re 1500

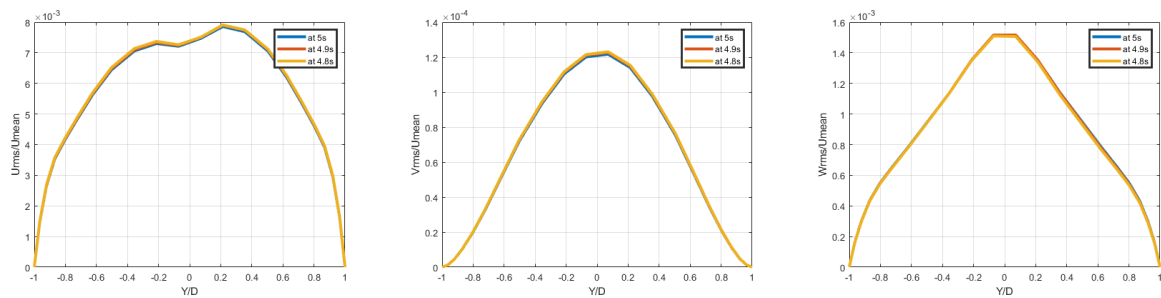


Figure 37: Temporal Convergence Rms Velocity profiles for Re 1500

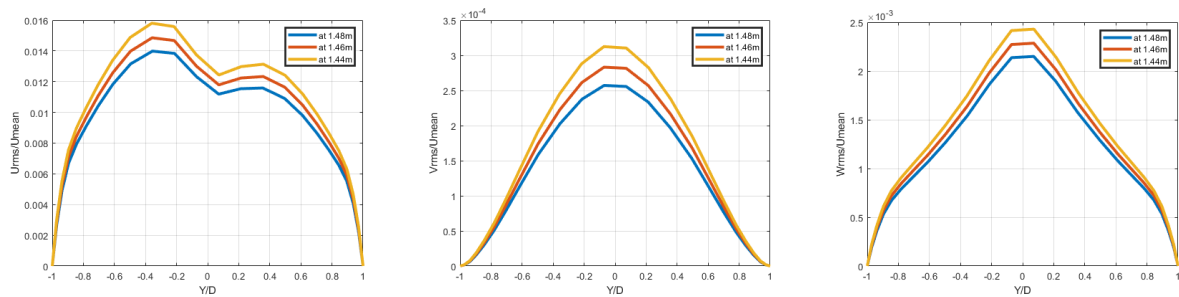


Figure 38: Spatial convergence of Rms Velocity profiles for Re 1800

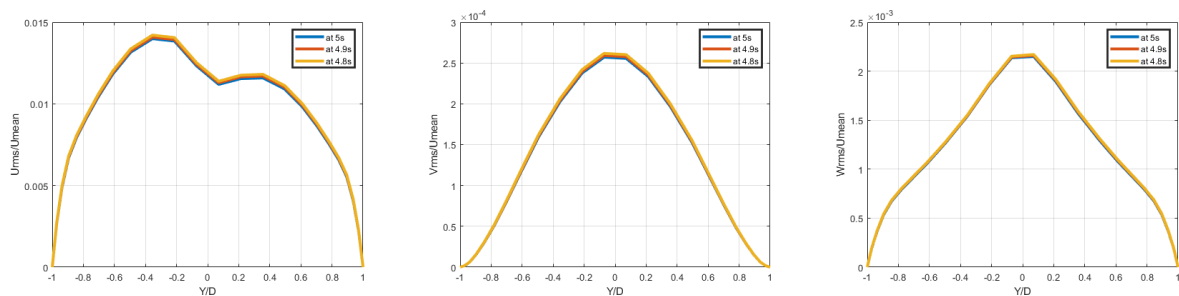


Figure 39: Temporal Convergence Rms Velocity profiles for Re 1800

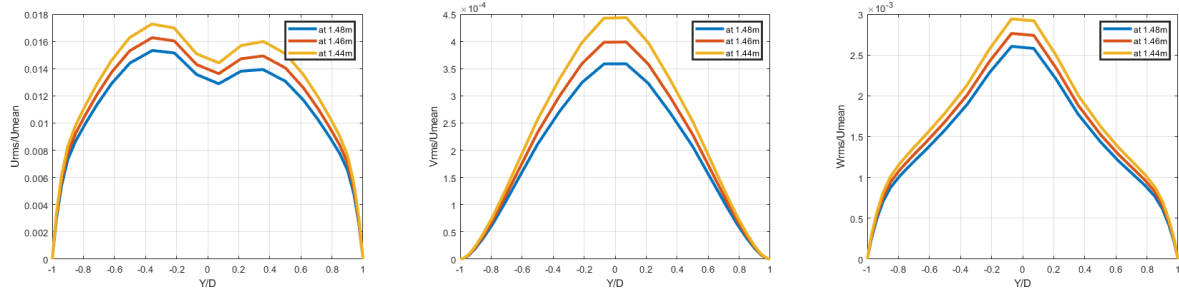


Figure 40: Spatial convergence of Rms Velocity profiles for Re 2000

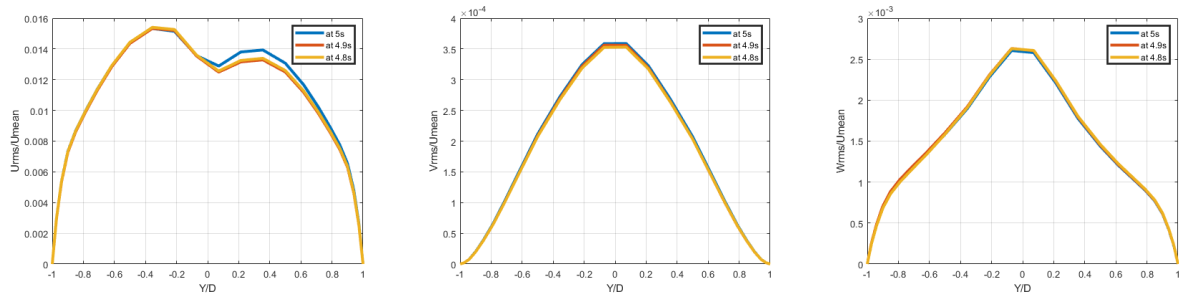


Figure 41: Temporal Convergence Rms Velocity profiles for Re 2000

Appendix-G

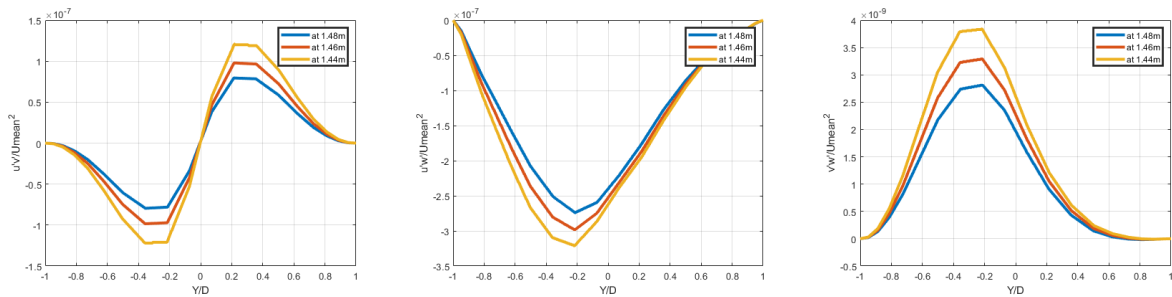


Figure 42: Spatial convergence of Turbulent Shear stress profiles for Re 1200

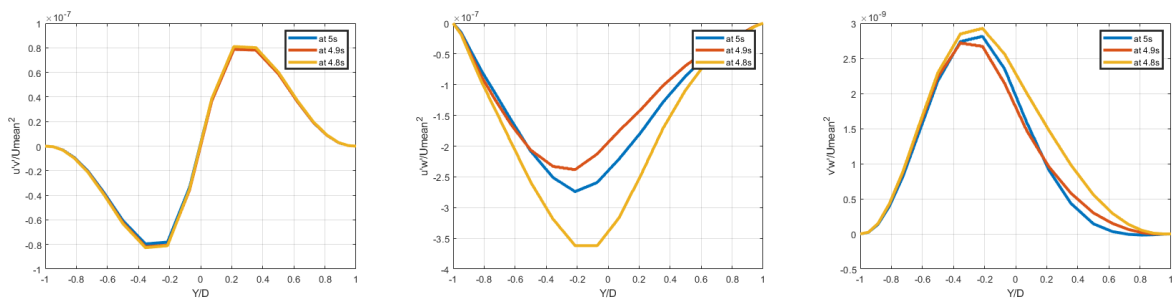


Figure 43: Temporal convergence of Turbulent Shear stress profiles for Re 1200

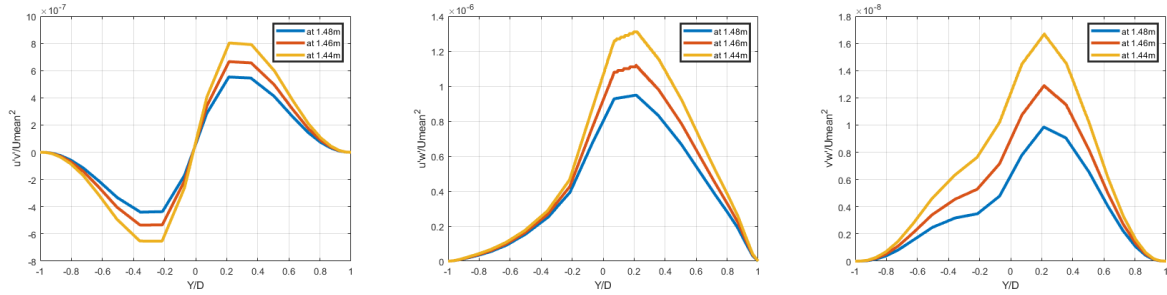


Figure 44: Spatial convergence of Turbulent Shear stress profiles for Re 1500

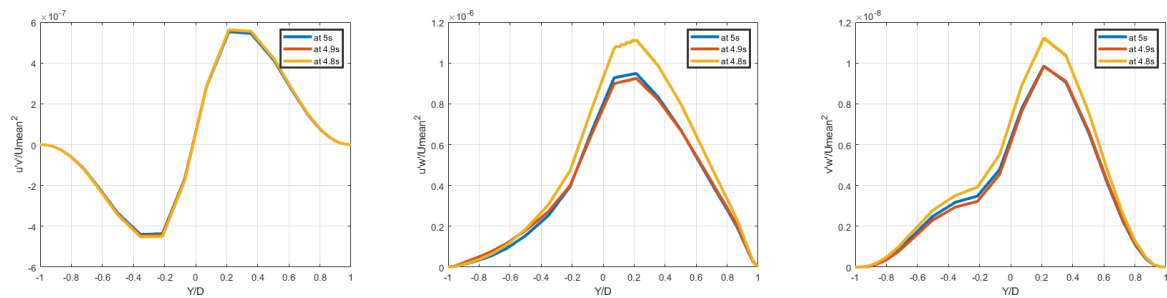


Figure 45: Temporal convergence of Turbulent Shear stress profiles for Re 1500

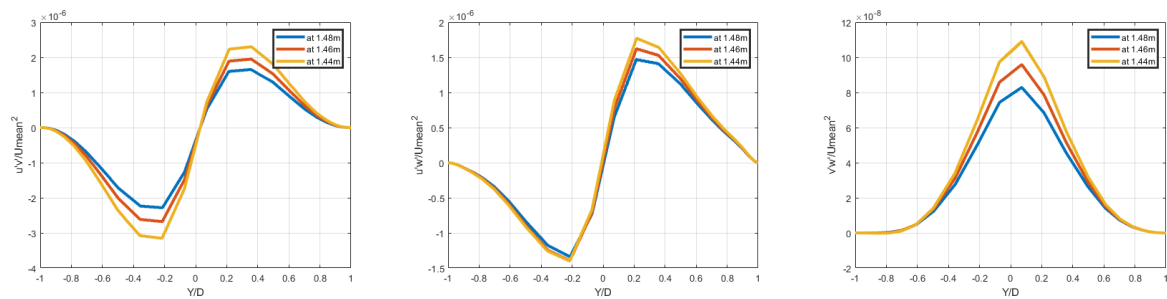


Figure 46: Spatial convergence of Turbulent Shear stress profiles for Re 1800

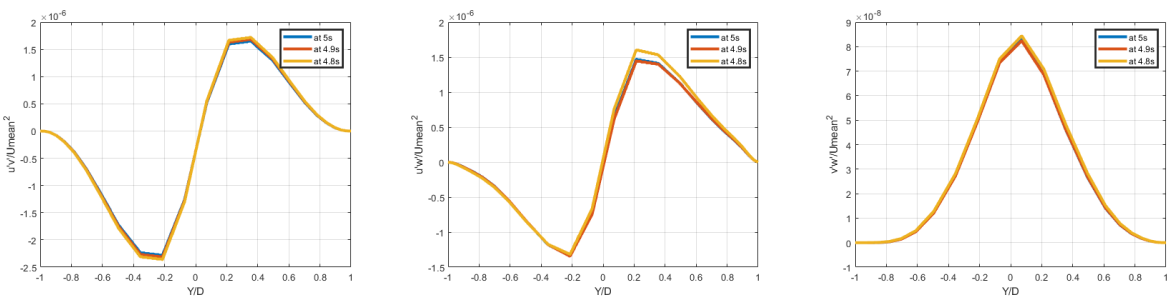


Figure 47: Temporal convergence of Turbulent Shear stress profiles for Re 1800

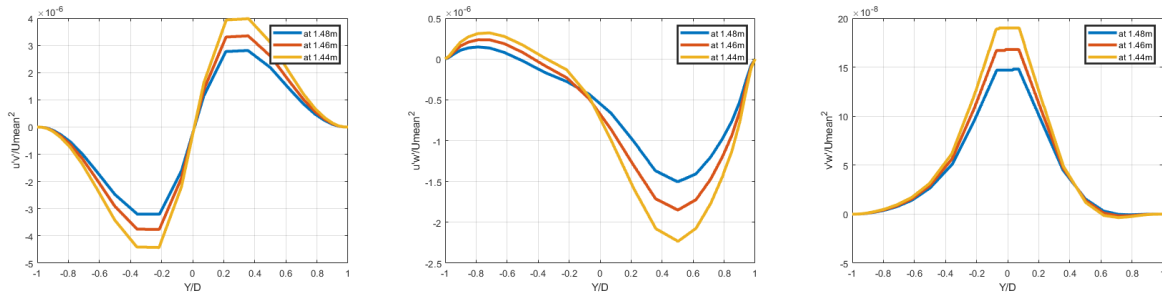


Figure 48: Spatial convergence of Turbulent Shear stress profiles for Re 2000

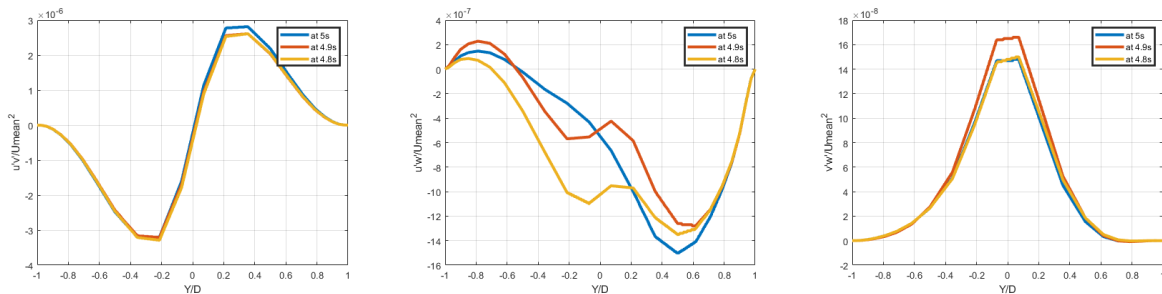


Figure 49: Temporal convergence of Turbulent Shear stress profiles for Re 2000

7 References

Gohil, T. B., Saha, A. K., Muralidhar, K. (2014). Large eddy simulation of a free circular jet. *Journal of Fluids Engineering*, 136(5).

Gohil, T. B., Saha, A. K., Muralidhar, K. (2011). Direct numerical simulation of naturally evolving free circular jet. *Journal of fluids engineering*, 133(11).

Pope, S. B. (2001). *Turbulent flows*.

Poletto, R., Craft, T., Revell, A. (2013). A new divergence free synthetic eddy method for the reproduction of inlet flow conditions for LES. *Flow, turbulence and combustion*, 91(3), 519-539.

Xu, H., Khalid, M., Pollard, A. (2003). Large eddy simulation of turbulent flow in a confined square coaxial jet. *International Journal of Computational Fluid Dynamics*, 17(5), 339-356.

<http://www.physics.drexel.edu/valliere/PHYS305/MonteCarlo/randomnumber//s/gaussianpoints.c>

Zhang, Y. (2017). Critical transition Reynolds number for plane channel flow. *Applied Mathematics and Mechanics*, 38(10), 1415-1424.

Kundu, B., Simlandi, S., Das, P. K. (2011). Analytical techniques for analysis of fully devel-

oped laminar flow through rectangular channels. Heat and mass transfer, 47(10), 1289-1299.